

Thermal Radiation from Neutron Stars: Chandra Results

G.G. Pavlov¹, V.E. Zavlin² and D. Sanwal¹

¹ The Pennsylvania State University, 525 Davey Lab., University Park, PA 16802, USA

² Max-Planck-Institut für extraterrestrische Physik, Giessenbachstraße, 85748 Garching, Germany

Abstract. The outstanding capabilities of the *Chandra* X-ray observatory have greatly increased our potential to observe and analyze thermal radiation from the surfaces of neutron stars (NSs). Such observations allow one to measure the surface temperatures and confront them with the predictions of the NS cooling models. Detection of gravitationally redshifted spectral lines can yield the NS mass-to-radius ratio. In rare cases when the distance is known, one can measure the NS radius, which is particularly important to constrain the equation of state of the superdense matter in the NS interiors. Finally, one can infer the chemical composition of the NS surface layers, which provides information about formation of NSs and their interaction with the environment. We will overview the recent *Chandra* results on the thermal radiation from various types of NSs – active pulsars, young radio-quiet neutron stars in supernova remnants, old radio-silent “dim” neutron stars – and discuss their implications.

1. Introduction

Observational study of thermal emission from isolated (non-accreting) neutron stars (NSs) became possible after the launch of *Einstein* (1979) and *EXOSAT* (1983), the first X-ray observatories equipped with X-ray telescopes. Contrary to nonthermal radiation of NSs, generated in the pulsar magnetospheres and observed from radio to γ -rays, thermal emission originates immediately at the surface, with the bulk of the energy flux in the soft X-ray band. Therefore, comparing the spectra and the light curves with the models for NS thermal radiation (see the contribution by Zavlin & Pavlov in these Proceedings; ZP02 hereafter), one can infer the NS surface temperature, magnetic field, gravitational acceleration, and chemical composition, as well as the NS mass and radius. The analysis of such observations allows one to trace thermal evolution of NSs (Tsuruta 1998) and constrain the properties of the superdense matter in the NS interiors (D.G. Yakovlev et al., these Proceedings).

Observational manifestations of NSs are very diverse, and only some of these exotic objects are suitable for ob-

serving the NS thermal emission. Most of the *detected* NSs are radio pulsars. Very young, active pulsars (with ages $\tau \lesssim 10^3$ yr — e.g., the Crab pulsar) are quite hot, with expected surface temperatures ~ 1 –2 MK, but their non-thermal radiation is so bright that the thermal radiation is hardly observable. The nonthermal component in X-ray emission of middle-aged pulsars ($\tau \sim 10^4$ – 10^6 yr — e.g., B0656+14, B1055–52) is much fainter, and their thermal radiation, with temperatures 0.3–1 MK, can dominate at soft X-ray and UV energies. The surfaces of old pulsars ($\tau \gtrsim 10^6$ yr — e.g., B0950+08, B1929+10, J0437–4715) are too cold to be seen in X-rays, but their polar caps are expected to be heated up to a few million kelvins, hot enough to emit observable thermal X-ray radiation.

In addition to active pulsars, a number of radio-quiet isolated NSs emitting thermal-like X-rays have been detected, with typical temperatures ~ 0.5 –5 MK. They are usually subdivided in four classes: Anomalous X-ray Pulsars (AXPs; see S. Mereghetti et al., these Proceedings), Soft Gamma-ray Repeaters (SGRs; Kouveliotou 1995), “dim” or “truly isolated” radio-silent NSs (i.e., not associated with supernova remnants [SNRs]; Treves et al. 2000), and compact central sources (CCOs) in SNRs (Pavlov et al. 2002a) which have been identified with neither active pulsars nor AXPs/SGRs. Their observational manifestations (particularly, multiwavelength spectra) are quite different from those of “active” pulsars, and their properties have not been investigated as extensively, but the presence of the thermal component in their radiation provides a clue to understand the nature of these objects.

First thermally emitting isolated NSs were detected with *Einstein* (e.g., Fahlman & Gregory 1981; Cheng & Helfand 1983; Helfand & Becker 1984; Seward, Charles, & Smale 1986; Córdoba et al. 1989) and investigated with *EXOSAT* (Brinkmann & Ögelman 1987; Kellett et al. 1987). In 1990’s, *ROSAT* and *ASCA* detected X-rays from more than 30 radio pulsars, including a few thermal emitters (Ögelman 1995), and discovered several radio-silent NSs (see Becker & Pavlov 2002 for a review). Thermal emission from a few isolated NSs was also detected in the optical-UV range with the *Hubble Space Telescope* (e.g.,

Pavlov, Stringfellow & Córdova 1996; Walter & Matthews 1997).

The new era in observing X-ray emission from NSs has started with the launch of two currently operating X-ray observatories of outstanding capabilities, *Chandra* and *XMM-Newton*. In this review we present recent results on thermal X-ray emission from isolated NSs of various types observed with *Chandra*. A more general overview of *Chandra* observations of NSs is presented in this volume by M.C. Weisskopf, while the *XMM-Newton* results on NSs are reviewed by W. Becker.

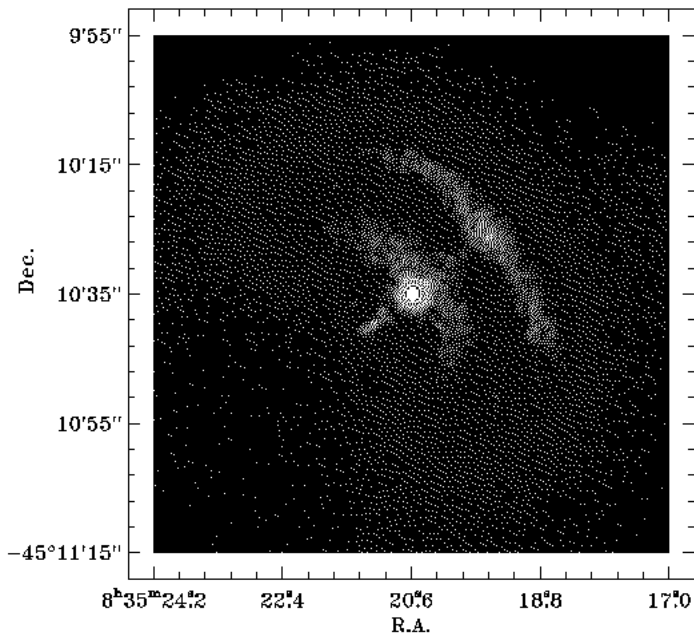


Fig. 1. *Chandra* HRC-I image of the Vela pulsar and surrounding nebula.

2. Thermal emission from radio pulsars

X-ray emission of rotation-powered pulsars generally consists of two components — thermal and nonthermal. The nonthermal component, generated by relativistic particles in the NS magnetosphere, is, as a rule, strongly pulsed and characterized by a power-law (PL) spectrum. Studying the magnetospheric component is important to understand the mechanisms of the multiwavelength (optical through gamma-rays) pulsar radiation. The thermal component, emitted from the NS surface, can be observed in X-rays if it is not buried under the nonthermal component, as in very young pulsars, and if the temperature is not too low, as in old pulsars. Weak pulsations of the thermal emission can be caused by temperature nonuni-

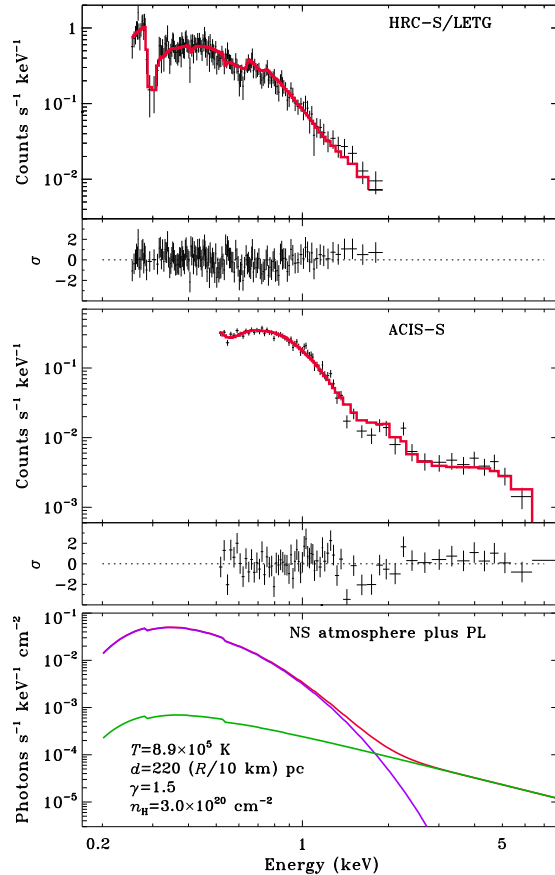


Fig. 2. Two-component (magnetic hydrogen NS atmosphere plus power law) model fit to the combined HRC-S/LETG and ACIS count rate spectra. The bottom panel shows the contributions from the thermal and nonthermal components (lilac and green lines, respectively).

formities along the NS surface and/or anisotropy of the radiation intensities in a strong magnetic field (see ZP02). Stronger pulsations of thermal radiation can be observed in old pulsars which emit thermal X-ray radiation from small, hot polar caps around the magnetic poles. In this Section we present the results of our analysis of *Chandra* data on pulsars of different ages: the young Vela pulsar ($\tau_c \equiv P/2\dot{P} = 11$ kyr), the middle-aged pulsars B0656+14 ($\tau_c = 110$ kyr) and B1055-52 ($\tau_c = 500$ kyr), and the very old millisecond pulsar J0437-4715 ($\tau_c = 4.9$ Gyr).

2.1. The Vela pulsar

First *Chandra* observations of this famous 89-ms radio, optical and γ -ray pulsar in the Vela SNR (the distance $d \approx 300$ pc — Caraveo et al. 2001) were carried out with the imaging array of the High Resolution Camera (HRC-I) in January and February 2000. These observations revealed a very complicated structure of the PWN around the pulsar (see Fig. 1) studied by Helfand, Halpern & Got-

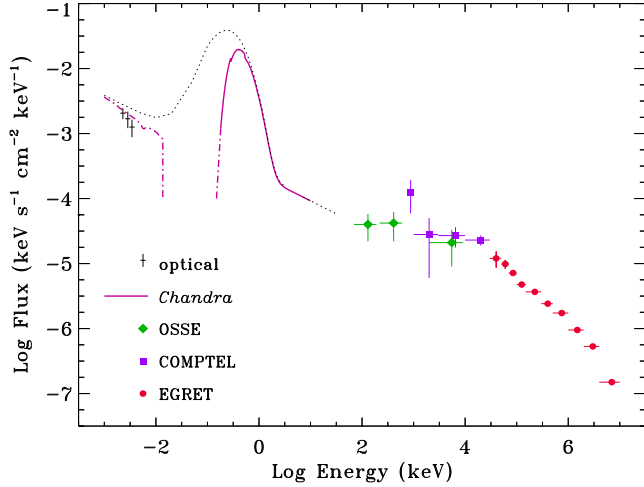


Fig. 3. Multiwavelength energy spectrum of the Vela pulsar. The solid line shows the NS atmosphere plus PL fit to the observed LETG and ACIS spectra. The dotted line corresponds to same model spectrum corrected for the interstellar absorption and extrapolated to lower and higher energies. The dash-dot lines show the extrapolated optical and EUV absorbed spectra (see Pavlov et al. 2001b for details and references).

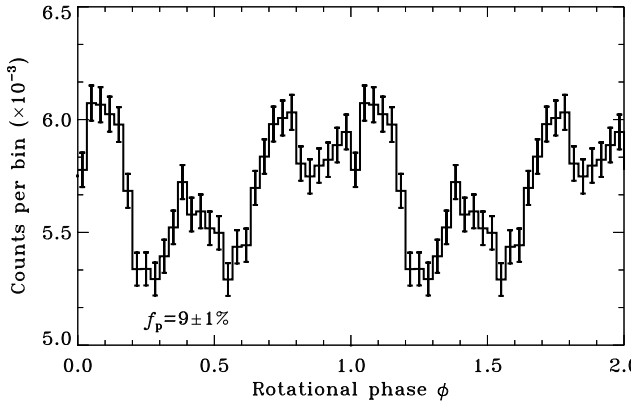


Fig. 4. Light curve of the Vela pulsar from two HRC-I observations of January and February 2000. The zero phase corresponds to the radio peak.

thelf (2001) and Pavlov et al. (2000, 2001a). The superb spatial resolution of *Chandra* made it possible, for the first time, to resolve the pulsar from its surroundings and investigate the pulsar’s radiation.

The spectral data on the Vela pulsar were obtained in two observations (Pavlov et al. 2001b). A 25 ks HRC-S observation with Low Energy Transmission Grating (LETG) of January 2000 provided the high-resolution pulsar spectrum in the energy range $E = 0.25\text{--}2.0$ keV. The analysis of the LETG spectrum ($\approx 7,000$ source counts) did

not reveal statistically significant spectral lines. The spectrum is best fitted with thermal models (blackbody, hydrogen NS atmosphere), but the observed spectrum somewhat exceeds the model spectra at $E \gtrsim 1.5$ keV (see upper panel in Fig. 2), indicating the presence of a second component with a harder spectrum. The spectrum at higher photon energies was provided by a 37 ks observation (October 1999) with the Advanced CCD Imaging Spectrometer (ACIS), taken in the Continuous Clocking (CC) mode that allows timing at the expense of imaging capability in one dimension. The 1-D count distributions of the pulsar and the nebula show that the pulsar is much brighter than the PWN background at $E \lesssim 1.5$ keV, and it is discernible up to 8 keV, where the charged particle background takes over (see Fig. 1 in Pavlov et al. 2001b). The pulsar spectrum in the 0.5–8 keV band ($\approx 9,000$ source counts) does not fit one-component models, but it fits fairly well two-component models (e.g., a PL plus a thermal component — see the middle panel in Fig. 2).

The analysis of the combined (LETG plus ACIS) spectra proves that the pulsar’s soft X-ray emission, at $E \lesssim 1.8$ keV, is indeed dominated by a thermal component (see bottom panel in Fig. 2). The parameters of this component are drastically different for the blackbody fit ($T_{\text{bb}}^{\infty} = 1.4\text{--}1.5$ MK, $R_{\text{bb}}^{\infty} = [2.3\text{--}2.9] d_{300}$ km) and the NS hydrogen atmosphere fit ($T_{\text{eff}}^{\infty} = 0.65\text{--}0.71$ MK, $R^{\infty} = [17\text{--}20] d_{300}$ km). Such strong difference is explained by the fact that the spectrum of a hydrogen atmosphere decreases with increasing photon energy slower than the ideal Wien spectrum because the radiation at higher energies comes from hotter layers. As a result, the blackbody fit to a hydrogen atmosphere spectrum yields a temperature higher than the true effective temperature and an area smaller than the true emitting area (see ZP02 for more details).

The small blackbody radius might hint that the observed radiation is emitted from hot spots (e.g., polar caps heated by relativistic particles produced in the pulsar magnetosphere), whereas the radius obtained in the hydrogen atmosphere fit implies radiation emitted from the entire NS surface. Rigorously speaking, the surface (atmosphere) of a NS is not a black body, but a blackbody spectrum could mimic the spectrum of a heavy-element (e.g., iron) atmosphere if it is observed with low spectral resolution. However, the lack of significant spectral lines in the LETG spectrum indicates that there are no heavy elements, neither He nor metals, in the radiating atmospheric layers. On the other hand, even strongly magnetized hydrogen does not have spectral features in the investigated energy band (all the hydrogen features are below 0.17 keV for the field of $B = 3 \times 10^{12}$ G, adopted for the Vela pulsar). Therefore, the hydrogen atmosphere interpretation looks more plausible. With this interpretation, the effective temperature of the Vela pulsar is well below the predictions of the “standard” models of the NS cooling (e.g., Tsuruta 1998).

An important result of this analysis is the detection of the hard spectral component which dominates at $E \gtrsim 1.8$ keV. The slope (photon index) of this PL component is $\gamma = 1.2$ – 1.8 if the NS hydrogen atmosphere model is adopted for the soft component. With this interpretation, the overall X-ray spectrum of the the Vela pulsar is quite similar to those of the three middle-aged pulsars, Geminga, B1055–52 and B0656+14 (see below), where the thermal component was detected, although the ratio of the nonthermal X-ray luminosity to the spin-down energy loss rate, $L_x/\dot{E} \simeq 3 \times 10^{-6}$ in the 0.2–8.0 keV range, is a factor of 10^3 smaller than observed for typical X-ray detected pulsars (Becker & Trümper 1997). If the L_x/\dot{E} ratio were as high as for other pulsars, the thermal radiation would be undetectable in the phase-integrated spectrum.

It is illuminating to compare the nonthermal X-ray spectrum of the pulsar with those in other energy ranges. Figure 3 shows the spectral flux of the pulsar from optical to gamma-rays. Remarkably, the extrapolation of the PL spectrum obtained in the atmosphere-plus-PL fit matches fairly well with the optical and hard-X-ray (soft- γ -ray) time-averaged fluxes. Moreover, under the hypothesis that the PL spectrum has the same slope in the optical through X-ray range, we can constrain the photon index very tightly: $\gamma = 1.35$ – 1.45 .

The multicomponent structure of the pulsar radiation is also seen from its pulse profile. The HRC-I light curve is shown in Figure 4 (see also Helfand et al. 2001; Sanwal et al. 2002a). It has at least three peaks — quite unusual for a pulsar, but not so surprising for the Vela pulsar which shows up to four peaks in the hard X-ray bands observed with *RXTE* (Harding et al. 2002).

So far, only the analysis of phase-integrated spectra and energy-integrated light curves has been possible. Phase-resolved spectral analysis and energy-resolved timing would be of crucial importance to elucidate the complicated emission mechanism(s) of both the nonthermal and thermal components. In particular, the analysis of the phase-energy dependence of the thermal emission, based on the NS atmosphere models can make it possible to determine the surface distributions of the temperature and the magnetic field.

2.2. Middle-aged pulsars B0656+14 and B1055–52

Among about 40 rotation-powered pulsars detected with the previous and currently operating X-ray missions, middle-aged pulsars ($\tau \sim 0.1$ – 1 Myr) are of special interest because their thermal emission is expected to dominate in soft X-rays. The best studied objects of this class are the “Three Musketeers”¹: PSR B0656+14, Geminga, and PSR B1055–52.

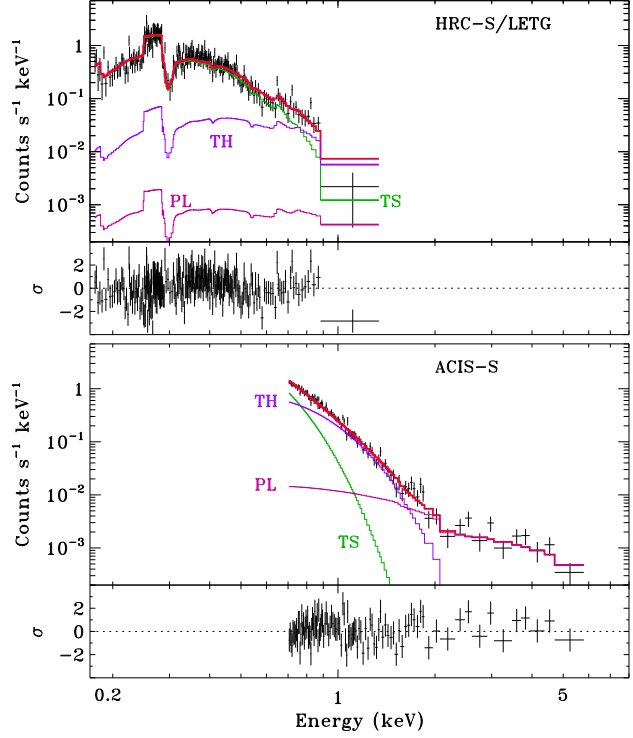


Fig. 5. Three-component, TS+TH+PL, fit to the combined LETG and ACIS-S spectra of PSR B0656+14. The red curves show the model countrate spectra for the two instruments.

2.2.1. PSR B0656+14

PSR B0656+14 ($\tau_c = 110$ kyr) is the brightest of the Three Musketeers. Observations with *Einstein*, *ROSAT*, and *ASCA* have shown that its X-ray spectrum consists of at least two components. The thermal component ($E \lesssim 1$ keV) resembles a soft blackbody spectrum with an apparent temperature of about 0.9 MK. Because of the narrow energy band of *ROSAT* and poor angular resolution of *ASCA*, the shape of the hard component (at $E \gtrsim 1$ keV) could hardly be determined from those data. For instance, the *ASCA* spectra above 1 keV can be fitted equally well with a hard blackbody with temperature of about 2.5–4.0 MK or a PL with photon index $\gamma = 1.3$ – 3.0 . IR-optical-UV observations of the pulsar (Pavlov et al. 1997; Koptsevich et al. 2001) revealed a nonthermal PL component with $\gamma = 1.4$ – 1.5 , presumably emitted from the pulsar magnetosphere.

To search for spectral features in the X-ray spectrum of PSR B0656+14 and investigate the shape of its high-energy tail, the pulsar was observed with HRC-S/LETG in November 1999 (38 ks exposure) and ACIS-S (in CC mode) in December 2001 (25 ks exposure). The analysis of these data showed no significant features in the source spectrum. To obtain a good fit to the combined X-ray spectrum in the 0.2–6 keV band, a three-component model is required. The high-energy tail ($E \gtrsim 2$ keV) fits

¹ As dubbed by J. Trümper

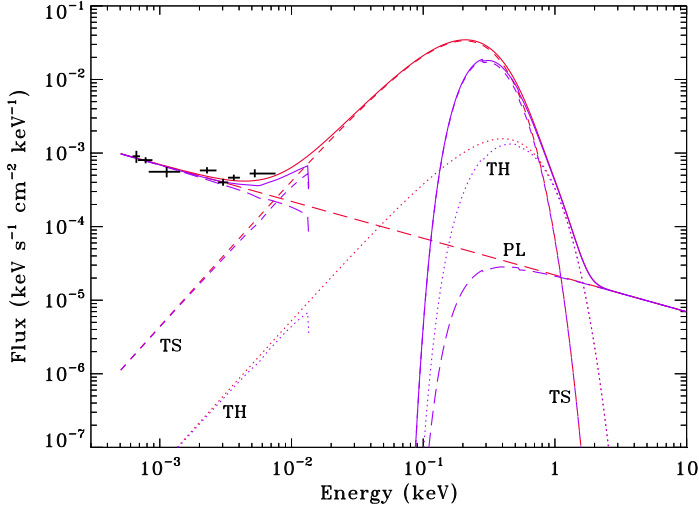


Fig. 6. Spectral flux for the TS+TH+PL model for PSR B0656+14 extrapolated to the optical range. Blue and red curves show the absorbed and unabsorbed spectra, respectively. Crosses are the IR-optical-UV fluxes (Koptsevich et al. 2001).

best with a PL spectrum with a slope close to that of the optical spectrum. To constrain it more tightly, we assumed that the slope does not change from optical to X-rays, included the optical data in the fit, and obtained $\gamma = 1.5$. The low-energy part of the spectrum ($E \lesssim 0.7$ keV) fits well with a blackbody spectrum with temperature $T_s^\infty = 0.85$ MK and equivalent radius of emitting sphere $R_s^\infty = 12.0 (d/500 \text{ pc})$ km. This thermal soft (TS) component is presumably emitted from the whole visible NS surface. To fit the spectrum at intermediate energies, one more component is required (see Fig. 5). Very likely, this is a thermal hard (TH) component with temperature $T_h^\infty \simeq 1.65$ MK (as given by the blackbody model) emitted from pulsar’s polar caps of radius $R_{\text{pc}} = R_h^\infty \simeq 1.0 (d/500 \text{ pc})$ km heated by relativistic particles streaming down from the pulsar acceleration zones. The bolometric luminosity of the TS component is $L_{\text{bol,s}} \simeq 5.5 \times 10^{32} (d/500 \text{ pc})^2 \text{ erg s}^{-1}$, vs. $L_{\text{bol,h}} \simeq 4.9 \times 10^{31} (d/500 \text{ pc})^2 \text{ erg s}^{-1}$ for the TH component. The luminosity of the nonthermal component is $L_x \simeq 5.3 \times 10^{30} (d/500 \text{ pc})^2 \text{ erg s}^{-1}$ in the 0.1–10.0 keV range. This three-component model fits the data from IR through X-ray energies (Fig. 6).

Using the magnetic hydrogen atmosphere models (ZP02), instead of blackbodies, for the thermal components gives formally acceptable fits, with effective temperatures lower by a factor of about 2 (e.g., $T_{\text{eff}}^\infty \simeq 0.4\text{--}0.5$ MK for the TS component). However, these fits imply either very small distances, $\sim 70\text{--}130$ pc for $R = 10$ km, or very large radii, $R_s \sim 40\text{--}70$ km for the TS component,

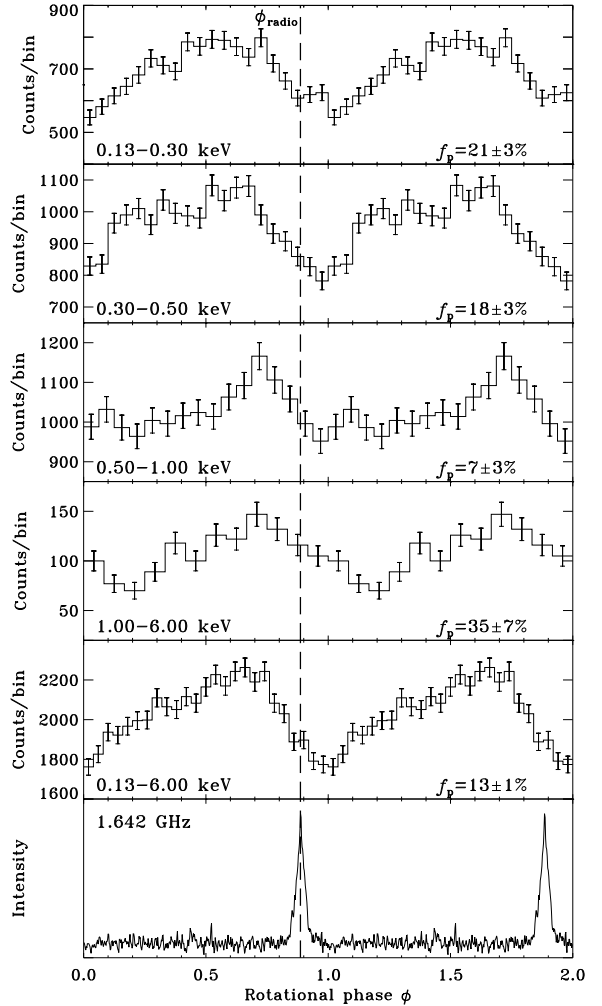


Fig. 7. X-ray pulse profiles for PSR B0656+14 in different energy bands (four upper panels). The radio pulse profile at 1.642 GHz (Gould & Lyne 1998) demonstrates the phase difference between the X-ray and radio peaks. The X-ray data are from the *Chandra* ACIS observation in the CC mode (December 2001).

at $d = 500$ pc. Therefore, applicability of these models to PSR 0656+14 is questionable.

The multicomponent structure of the pulsar X-ray radiation is also seen from the behavior of the pulse profiles shown in Figure 7. The shape of the light curves is energy dependent, with a significant phase shift (~ 0.2 of the period) at 0.5–0.7 keV. The source pulsed fraction f_p shows a complex behavior: it decreases with increasing energy from about 20% at $E \sim 0.1\text{--}0.3$ keV down to about 7% at E around 1 keV and increases again to $f_p \simeq 35\%$ at $E \gtrsim 1$ keV. The X-ray peak lags the radio peak by 0.2–0.4 of the period, depending on energy (Fig. 7).

To establish the origin of the peak and the parameters of the X-ray radiation, one should analyze the spec-

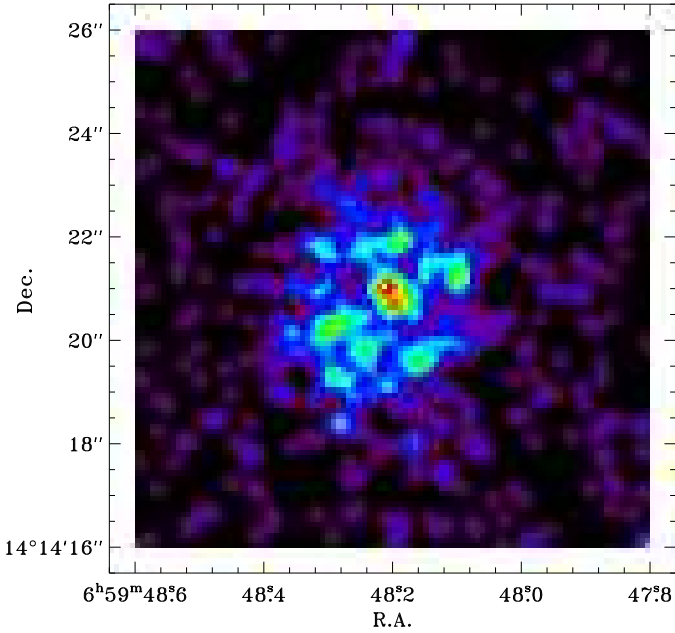


Fig. 8. Image of a $10'' \times 10''$ area around PSR B0656+14 from the 5 ks ACIS observation in the Timed Exposure mode (December 2001).

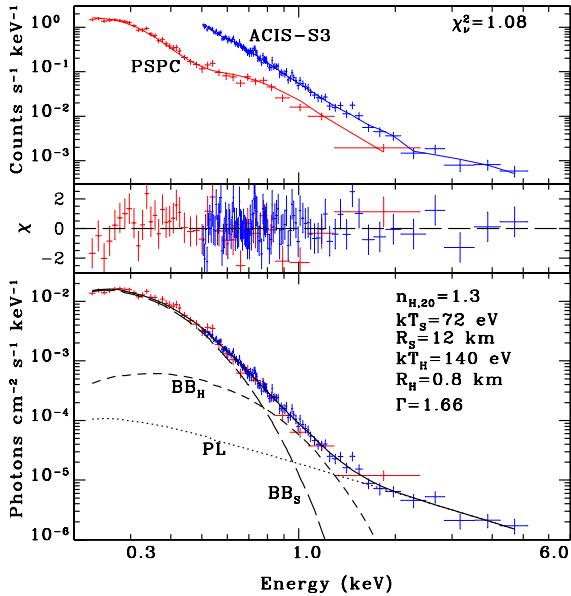


Fig. 9. Three-component model fit to the *Chandra* ACIS and *ROSAT* PSPC spectra of PSR B1055-52.

tra and the light curves together, with the aid of realistic models for X-ray emission. However, the spectra of the pulsar observed with the pre-*Chandra* X-ray observatories, and even the *Chandra* ACIS-S spectrum observed in

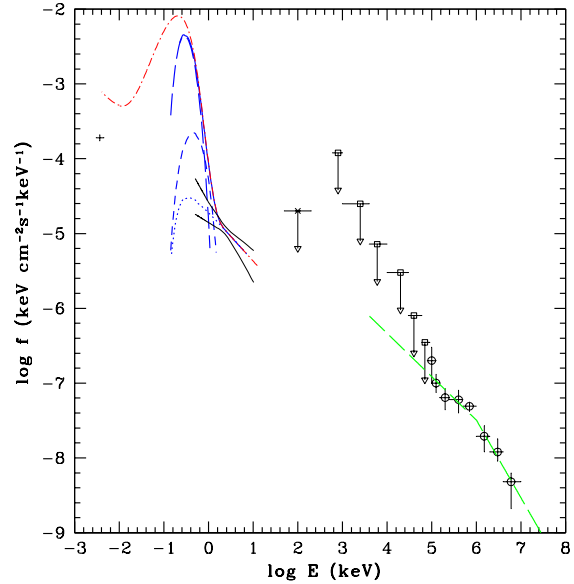


Fig. 10. Spectral flux from PSR 1055-52 for the TS+TH+PL model extrapolated to the optical and γ -ray ranges, together with the data from *HST*, *OSSE*, *COMPTEL* and *EGRET*. The blue and the red curves give the absorbed and unabsorbed spectra, respectively.

CC mode, potentially have a contaminating component — synchrotron radiation from a PWN of a small angular size around the pulsar, which could not be resolved in those observations.

A hint on extended emission around PSR 0656+14 is seen in the zero-order LETG/HRC-S image (Marshall & Schulz 2002), but that image is strongly contaminated by the diffraction spikes. The pulsar was also observed in a 5 ks exposure with ACIS-S3 in Timed Exposure mode (December 2001) providing the data for spatial analysis of the X-ray emission in the vicinity of the pulsar. The analysis reveals a $3''$ – $4''$ extended structure around the piled-up image of the pulsar — first strong indication on PWN around a middle-aged pulsar (see Fig. 8). The pulsar’s image, confined within a small, slightly elongated area of about $1''$ diameter (at the center of Fig. 8) is surrounded by a putative PWN of rather complicated morphology. The estimated luminosity of the PWN is $L_{x,pwn} \sim 2 \times 10^{31} (d/500 \text{ pc})^2 \text{ erg s}^{-1}$ in the 0.1–10.0 keV range. A considerable fraction of the PWN radiation can contaminate the pulsar’s radiation observed with the pre-*Chandra* observatories and even with ACIS in CC mode. Therefore, to unambiguously separate the PWN contribution, one should observe the pulsar and its surroundings in high-resolution imaging mode for longer time. The above estimates of the pulsar spectral parameters should be considered with caution until the properties of the putative PWN are studied and its radiation is separated from that of the pulsar.

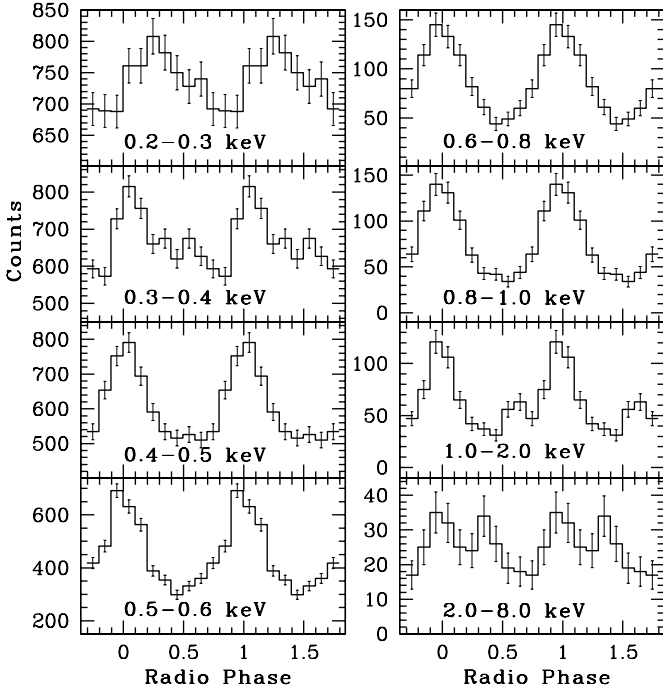


Fig. 11. Energy-resolved light curves of PSR B1055–52 plotted vs. radio phase.

2.2.2. PSR B1055–52

Analysis of the *Chandra* data on PSR B1055–52, taken in January 2000 with ACIS-S in CC mode (42 ks exposure), yields results very similar to those obtained for PSR B0656+14 (see Sanwal et al. 2002c for details). First, the ACIS spectrum, combined with that obtained with the *ROSAT* PSPC, requires a three-component model (Fig.

9). The high-energy tail of the spectrum ($E \gtrsim 2$ keV) is best described with a PL with $\gamma = 1.66$; such a component smoothly connects optical (*HST* FOC) and gamma-ray (*CGRO* EGRET) data (Fig. 10). The spectrum at lower energies fits well with two thermal (blackbody) components, soft and hard. The best-fit model parameters to the phase-integrated spectrum are $T_s^\infty = 0.84$ MK and $R_s^\infty = 12.0$ ($d/1$ kpc) km for the soft thermal component, $T_h^\infty = 1.62$ MK and $R_h^\infty = 0.8$ ($d/1$ kpc) km for the hard thermal component, $n_H = 1.3 \times 10^{20}$ cm $^{-2}$.

The energy-resolved light curves of the pulsar derived from the ACIS data reveal energy-dependent variations in the pulsed fraction, the phase of the pulse, and the pulse shape (Fig. 11). In particular, the pulsed fraction increases from $\sim 15\%$ at about 0.3–0.4 keV to $\sim 50\%$ at $\gtrsim 1.0$ keV. For this pulsar, the X-ray pulse at $E \gtrsim 0.3$ keV is in phase with the main radio pulse, contrary to PSR B0656+14.

The phase-resolved spectroscopy shows small variations in the parameters of the soft thermal component, whereas the emitting area for the hard thermal component varies significantly with the rotational phase (R_h^∞ changes between about 0.5 and 1.5 km), which can be interpreted as changing projection of the hot spot area.

Thus, we see remarkable similarity in the X-ray properties of the two middle-aged pulsars, B0656+14 and B1055–52. Interestingly, the temperature of the soft thermal component is approximately the same for these pulsars, although the characteristic age, $\tau_c = P/2\dot{P}$, is a factor of 5 larger for B1055–52. A possible explanation of this fact is that these NSs have different properties (e.g., the mass of B1055–52 is lower — see D.G. Yakovlev et al., this volume). An alternative explanation is that the true age of a pulsar can be quite different from its characteristic age (see below), so that one should be very cautious comparing the NS cooling models with the observations of pulsars.

2.3. Millisecond pulsar J0437–4715

Millisecond (recycled) radio pulsars are distinguished from ordinary pulsars by their very short and stable periods, $P \lesssim 10$ ms, $\dot{P} \sim 10^{-20}$ s s $^{-1}$. They are presumably very old objects, with spin-down ages $\tau \sim 10^9$ – 10^{10} yr and low magnetic fields, $B \sim 10^8$ – 10^{10} G. Similar to ordinary pulsars, a millisecond pulsar can emit nonthermal X-rays from its magnetosphere. Additionally, thermal X-rays can be emitted from pulsars’ polar caps heated up to X-ray temperatures by relativistic particles generated in the pulsar acceleration zones.

At a distance $d \simeq 140$ pc, PSR J0437–4715 ($P = 5.75$ ms) is the nearest and brightest millisecond pulsar known at both radio and X-ray wavelengths. It is in a 5.74 d binary orbit with a low-mass white dwarf companion. Optical observations in H_α have revealed a bow-shock PWN, caused by the supersonic motion of the pulsar through the interstellar medium, with the bow-shock apex at about $10''$ south-east of the pulsar, in the direction of the pul-

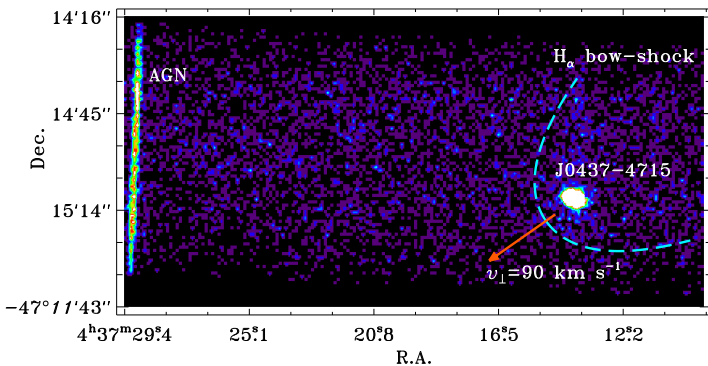


Fig. 12. ACIS image of PSR 0437–4715. The bright strip is the trailed image of a nearby AGN. The dashed curve marks the leading edge of the H_α bow-shock. The arrow shows the direction of the pulsar’s proper motion.

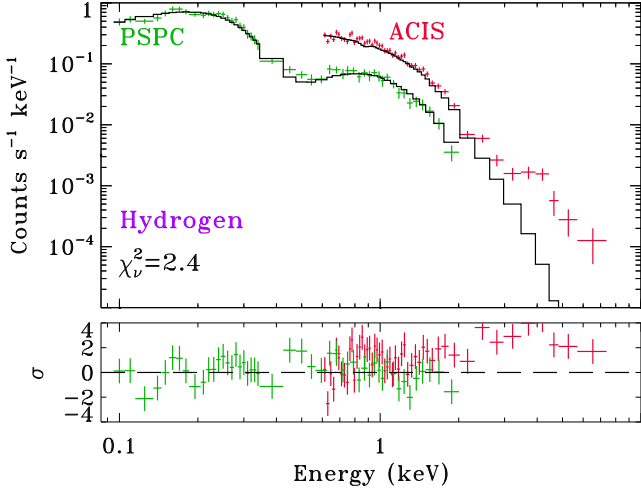


Fig. 13. Two-temperature hydrogen polar cap model fit to the combined ACIS and PSPC data on PSR J0437–4715.

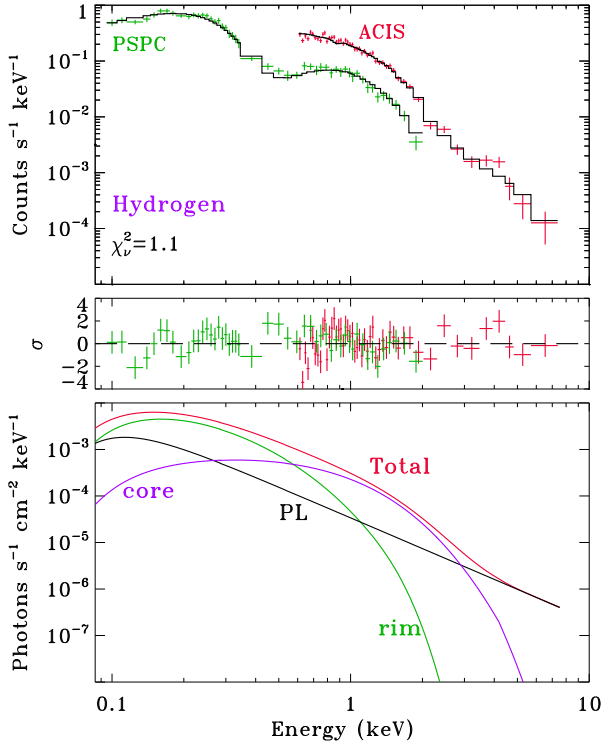


Fig. 14. Power-law plus two-temperature hydrogen polar cap model fit to the combined ACIS and PSPC spectrum of PSR J0437–4715.

sar’s proper motion. Its X-ray radiation was discovered with *ROSAT* (Becker & Trümper 1993). The pulsar was also observed with *EUVE* (Halpern, Martin, & Marshall 1996). The pre-*Chandra* data, obtained in a narrow energy range of 0.1–2.0 keV, can be well fitted with a PL with photon index $\gamma = 2.2$ –2.5, or with a polar cap model with

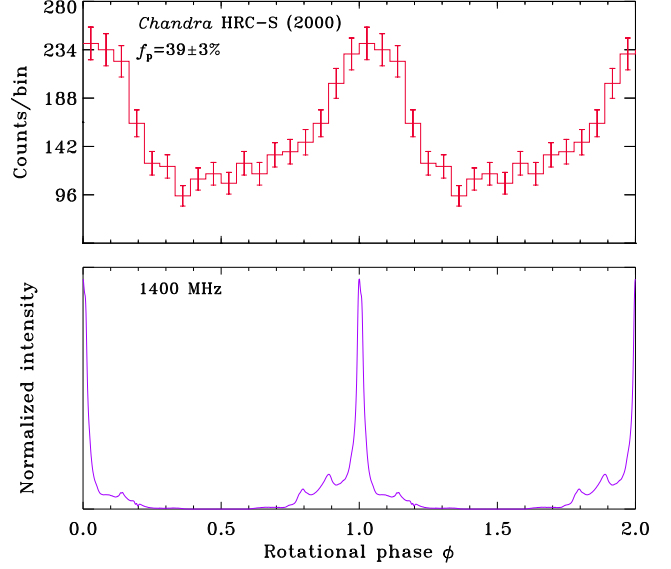


Fig. 15. Pulse profiles of PSR 0437–4715 from the *Chandra* and radio observations.

a nonuniform temperature distribution (Zavlin & Pavlov 1998 [ZP98]). To discriminate between these two competing models, the pulsar was observed with *Chandra* ACIS (May 2000; 26 ks exposure; see Zavlin et al. 2002).

The source spectrum prevails over background at energies up to 7 keV and reveals no significant spectral features. No structures which could be associated with the bow shock observed in H_α are found (see Fig. 12).

The combined analysis of the ACIS and *ROSAT* PSPC data rules out a single PL model (min $\chi_\nu^2 = 3.8$), indicating that more components are needed to get a satisfactory combined fit.

A two-component model, PL plus two polar caps of uniform temperature, provides an acceptable fit to the combined data. However, comparison with the *EUVE* data shows that this model is only marginally acceptable. In addition, the inferred values of hydrogen column density exceed the values $n_H = (1\text{--}3) \times 10^{19} \text{ cm}^{-2}$ derived from independent measurements of the interstellar absorption towards objects in the vicinity of the pulsar (see ZP98 for more details).

ZP98 suggested that the temperature distribution in a polar cap should be nonuniform because the heat, released by decelerating magnetospheric particles in sub-photospheric layers, propagates along the surface out from the small polar areas, where the energy is deposited, and heats a larger area. They used a two-zone approximation for the polar cap temperature distribution, a hot “core” plus a colder “rim”. When applied to the ACIS data, this model shows that the observed spectrum significantly exceeds the model at $E > 2$ keV, i.e., one more component is required (Fig. 13). A natural choice for the additional component is a PL. Adding the nonthermal component

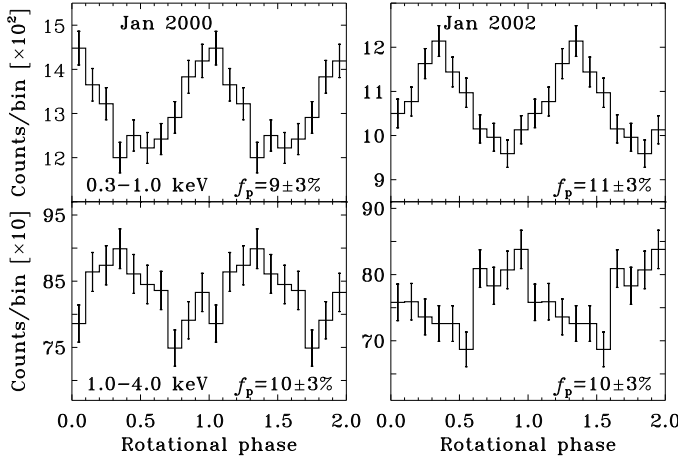


Fig. 16. Light curves of CXO J1210–5226 from two *Chandra* observations.

greatly improves the fit (Fig. 14). At fixed $n_{\text{H}} = 2 \times 10^{19} \text{ cm}^{-2}$, the best fitting parameters are $T_{\text{core}} = 2.1 \text{ MK}$, $T_{\text{rim}} = 0.54 \text{ MK}$, $R_{\text{core}} = 0.12 \text{ km}$, $R_{\text{rim}} = 2.0 \text{ km}$, and $\gamma = 2.2$. The bolometric luminosity of two polar caps is $L_{\text{bol}} = 2.3 \times 10^{30} \text{ erg s}^{-1} \sim 0.6 \times 10^{-3} \dot{E}$, and the PL luminosity in the 0.1–10 keV band is $L_{\text{x}} = 0.7 \times 10^{30} \text{ erg s}^{-1} \sim 0.2 \times 10^{-3} \dot{E}$. This model is in good agreement with the *EUVE* data.

In the polar cap model with temperature decreasing outwards from the cap center, the thermal component dominates between 0.1 keV and 2.5 keV, providing about 75% of the X-ray flux, while the PL component dominates outside this band. An important point here is that this model requires the thermal radiation to be emitted from a hydrogen (or helium) NS atmosphere. The high spectral resolution of the ACIS data rules out an atmosphere comprised of heavier chemical elements.

The pulsar was also observed with the HRC-S detector (October 2000; 20 ks exposure) in the timing mode that provides accurate timing results. Figure 15 presents the HRC-S and radio pulse profiles. The phases of the X-ray and radio pulses are found to be virtually the same — their difference (0.3% of the pulsar’s period) is smaller than the absolute timing accuracy of *Chandra*. This implies that, if the main contribution to the HRC-S band is due to the thermal polar cap radiation, then the radio emission must be generated close to the NS surface — e.g., the time difference of $< 0.1 \text{ ms}$ between the X-ray and radio phases corresponds to a distance of $< 30 \text{ km}$, much smaller than the light cylinder radius of 275 km.

3. Compact central objects in supernova remnants

Chandra has observed five CCOs. Their most important characteristics are listed in Table 1. Although some properties of CCOs (in particular, their spectra) are very similar to each other, it does not necessary mean that they represent a uniform class of objects. The most outstanding is J1617–5102 in RCW 103, with its highly variable flux (time scales hours to months), putative 6.6 hr period, and a possible optical counterpart ($J \simeq 22.3$). One can presume that this source is not a truly isolated NS (i.e., it is powered by accretion, at least in its high state), although it is not a standard accretion-powered pulsar. The other four CCOs have shown neither long-term variabilities nor indications of binarity. If, based on the observed spectra, we adopt a plausible hypothesis that their radiation is thermal and assume that it can be adequately described by the same spectral model (e.g., BB or hydrogen NS atmosphere), then we have to conclude that the emitting area is growing with age. If the radiation emerges from a hydrogen atmosphere, then the effective radius is consistent with a NS radius for two oldest CCOs, J0821–4300 and J1210–5226, being smaller for two youngest ones, J2323+5848 and J0852–4617. One might assume that the latter two are black holes, not NSs, but then one would have to invoke accretion as the energy source, which does not look consistent with the lack of variability.

A recent review on CCOs, including the *Chandra* results, has been presented by Pavlov et al. (2002a). Therefore, here we will describe only the most recent results on the best-investigated CCO, J1210–5226 (a.k.a. 1E 1207.4–5209), the first isolated NS which shows spectral lines.

3.1. J1210–5226: the puzzling pulsar in G296.5–10

This radio-quiet X-ray source at the center of G296.5+10.0 (a.k.a. PKS 1209–51/52) was discovered by Helfand & Becker (1984). Mereghetti, Bignami, & Caraveo (1996) and Vasisht et al. (1997) fitted the *ROSAT* and *ASCA* spectra of J1210–5226 with a blackbody model of $T_{\text{bb}}^{\infty} \simeq 3.0 \text{ MK}$ from an area with radius $R_{\text{bb}}^{\infty} \simeq 1.6 (d/2 \text{ kpc}) \text{ km}$. Zavlin, Pavlov & Trümper (1998) interpreted the observed spectra as emitted from a light-element (hydrogen or helium) atmosphere. For a NS of mass $1.4 M_{\odot}$ and radius 10 km, they obtained a NS surface temperature $T_{\text{eff}}^{\infty} = (1.4–1.9) \text{ MK}$ and a distance of 1.6–3.3 kpc, consistent with the distance to the SNR, $2.1_{-0.8}^{+1.8} \text{ kpc}$ (Giacani et al. 2000).

Zavlin et al. (2000) observed J1210–5226 with *Chandra* ACIS-S in CC mode in January 2000 (32 ks exposure) and discovered a period of about 424 ms, which proved that the source is a NS. Second *Chandra* observation with the same observational setup (January 2002; 30 ks) provided an estimate of the period derivative, $\dot{P} \sim (0.7–3) \times 10^{-14} \text{ s s}^{-1}$ (Pavlov et al. 2002b). This estimate im-

Object	Host SNR	Age kyr	Period	T_{bb}^{∞} MK	R_{bb}^{∞} km	$L_{\text{bol,bb}}^{\infty}$ 10^{33}erg s^{-1}	T_{eff}^{∞} MK	R^{∞} km	L_{bol}^{∞} 10^{33}erg s^{-1}
J2323+5848	Cas A	0.32	...	5.7	0.5	1.6	3.5	1	2
J0852-4617	G266.1-1.2	~ 1	301 ms [?]	4.6	0.3	0.3	3.1	1.5	0.8
J1617-5102	RCW 103	1-3	6.6 hr [?]	4.6-7.0	0.2-1.6	0.5-30	3.5	1-8	1-60
J0821-4300	Pup A	1-3	...	4.4	1.4	4.2	2.0	10	8
J1210-5226	G296.5+10.0	3-20	424 ms	2.9	1.6	1.3	1.6	11	1

Table 1. Compact central objects in SNRs with best-fit parameters for blackbody (columns 5–7) and hydrogen NS atmosphere models (columns 8–10). The periods marked with “[?]” require confirmation. More details on these objects can be found in Pavlov et al. (2002a).

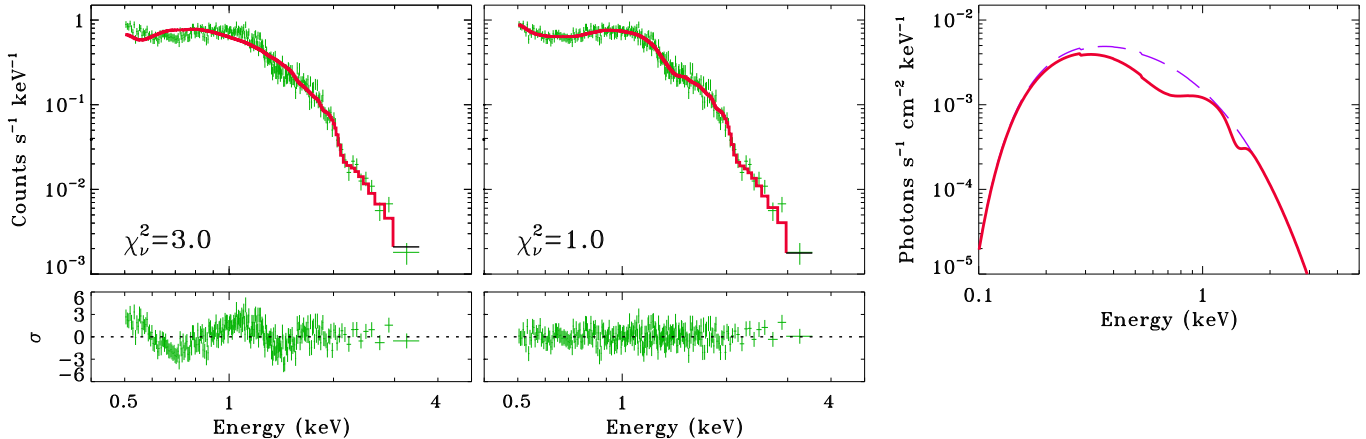


Fig. 17. *Left:* Fit to the *Chandra* spectrum of J1210-5226 with a blackbody model. *Middle:* The same model with two absorption lines added (at energies of 0.7 keV and 1.4 keV). Notice the significant improvement in the fit quality. *Right:* The two-line model for the photon flux (see text).

plies that the characteristic age of the NS, $\tau_c \sim 200$ –1600 kyr, is much larger than the 3–20 kyr age of the SNR (Roger et al. 1998), while the “canonical” magnetic field, $B \equiv 3.2 \times 10^{19} (P\dot{P})^{1/2} \text{ G} = (2-4) \times 10^{12} \text{ G}$, is typical for a radio pulsar. These observations revealed smooth pulsations of the X-ray flux from J1210-5226, with pulse shape depending on photon energy (Fig. 16).

The analysis of the ACIS spectra (Sanwal et al. 2002b) shows that continuum models (e.g., blackbody, power-law, fully ionized NS atmosphere) fail to fit the source spectrum, which deviates very significantly from any of the models, revealing two absorption features near 0.7 keV and 1.4 keV (Fig. 17). Including absorption lines in the spectral model improves the quality of the fit substantially. Assuming Gaussian profiles for the absorption coefficients, we obtain the central energies 0.73 ± 0.01 and 1.40 ± 0.01 keV, equivalent widths 108 ± 15 and 112 ± 24 eV, and central optical depths 0.40 ± 0.06 and 0.43 ± 0.06 , respectively.

Attempts to explain the absorption features as caused by the intervening interstellar (or circumstellar) material lead to huge overabundance for some elements. Therefore, the observed lines are most likely intrinsic to the NS.

One could assume that the observed lines are cyclotron lines produced in a strongly ionized NS atmosphere. If one assumes these are electron cyclotron lines, the features might be interpreted as the fundamental and the first harmonic of the electron cyclotron energy $E_{ce} = 1.16 B_{11} \text{ keV}$ in a magnetic field $B_{11} \equiv B/(10^{11} \text{ G}) \sim 0.6(1+z)$ (z is the neutron star redshift parameter), or as two fundamentals emitted from two regions with different magnetic fields, $B_{11} = 0.6(1+z)$ and $1.2(1+z)$, broadened by the radiative transfer effects and/or nonuniformity of the magnetic field. However, it is difficult to reconcile this interpretation with the expected strength of the surface magnetic field $B > 3 \times 10^{12} \text{ G}$. In addition, the oscillator strength of the first harmonic is smaller than that of the fundamental by a factor of $\sim E_{ce}/(m_e c^2) \sim 2 \times 10^{-3}$ (at $E_{ce} \gg kT$), so that it is hard to explain why the 1.4 keV feature is as

Object	T_{bb}^{∞} MK	f_x^a	n_{H} 10^{20} cm^{-2}	Period s	B mag	Ref.
RX J1856.5–3754	0.7	14	1.3	...	25.8	1
RX J0720.4–3125	0.9	11	1.1	8.37	26.6	2,3
RX J1605.3+3249	1.1	9	1.1	...	> 25	4
RX J0806.4–4123	0.9	3	2.5	11.37[?]	> 24	5,6
RX J0420.0–5022	0.7	1	1.7	22.69[?]	> 25.2	7
RX J1308.8+2127	1.4	5	2.1	5.16	> 26	8,9
RX J2143.0+0654	1.1	9	4.6	...	> 22.8 ^b	10

Table 2. Main properties of the seven “dim” NSs discovered with *ROSAT*. The spectral parameters are obtained from blackbody fits to the *ROSAT* PSPC data. The periods marked with “[?]” require confirmation.

Refs.: 1 - Walter et al. (1996); 2 - Haberl et al. (1997); 3 - Kulkarni & van Kerkwijk (1998); 4 - Motch et al. (1999); 5 - Haberl et al. (1998); 6 - Haberl & Zavlin (2002); 7 - Haberl et al. (1999); 8 - Schwobe et al. (1999); 9 - Hambaryan et al. (2001); 10 - Zampieri et al. (2001).

^a Absorbed flux in 0.1–2.0 keV, in units of $10^{-12} \text{ erg cm}^{-2} \text{ s}^{-1}$.

^b R magnitude.

strong as the 0.7 keV feature if we assume the two lines are associated with the same magnetic field.

One can assume that the spectral features are associated with ion cyclotron energies, $E_{ci} = 0.63(Z/A)B_{14}$ keV, where Z and A are the ion’s charge and mass numbers. The surface magnetic field needed for this interpretation is $\gtrsim 10^{14}$ G, much larger than the conventional magnetic field inferred for a centered dipole from the P , \dot{P} measurements. Such a strong *surface* magnetic field can be consistent with the magnetic moment $\mu = 3 \times 10^{30}$ G cm^3 if the magnetic dipole is off-centered to about 3 km below the surface. However, the ion-cyclotron interpretation of the observed features is not straightforward even in this case (see Sanwal et al. 2002b for more details).

Thus, the most viable possibility is that the observed lines are atomic lines formed in the NS atmosphere. The features cannot be explained as emerging from a hydrogen atmosphere because, at any magnetic field and any reasonable gravitational redshift, there is not a pair of strong hydrogen spectral lines whose energies would match the observed ones. Pavlov et al. (2002c) suggest that these are the strongest lines of once-ionized helium in a superstrong magnetic field, $(1.4\text{--}1.7) \times 10^{14}$ G. In this interpretation, the observed line energies correspond to the gravitational redshift $z = 0.12\text{--}0.23$, which corresponds to $R/M = 8.8\text{--}14.2 \text{ km } M_{\odot}^{-1}$. To confirm this result, deep observations with high spectral resolution are needed.

4. “Dim” isolated neutron stars

ROSAT discovered seven objects which are often called “dim” or “truly isolated” NSs. These sources, listed in Table 2, are characterized by blackbody-like spectra with temperatures around 1 MK. Low values of hydrogen column densities, $n_{\text{H}} \sim 10^{20} \text{ cm}^{-2}$, suggest small distances to these objects. Their X-ray fluxes, $f_x \sim 10^{-12}\text{--}10^{-11} \text{ erg s}^{-1} \text{ cm}^{-2}$, correspond to rather low (bolometric) luminosities, $L \sim 10^{30}\text{--}10^{31} \text{ erg s}^{-1}$ for a fiducial distance of 100 pc. The fluxes do not show variations on either short

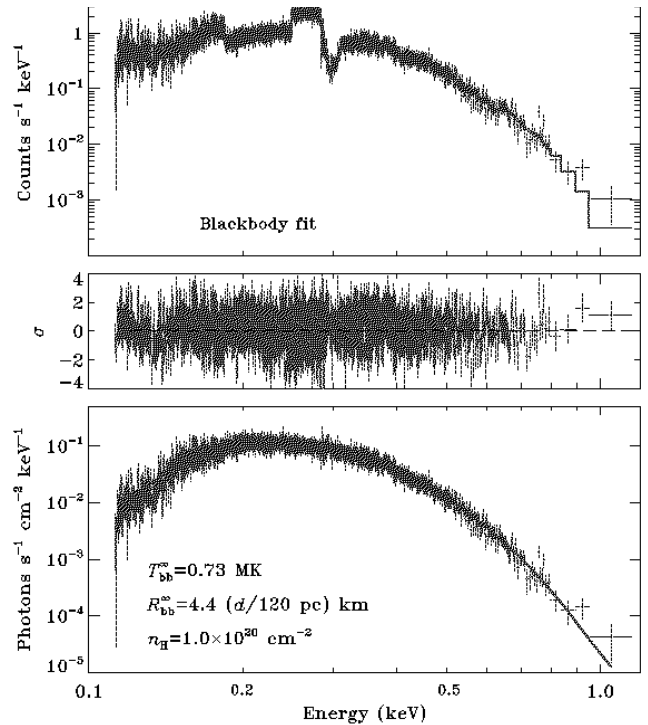


Fig. 18. *Chandra* LETG/HRC-S spectrum of RX J1856.5–3754 collected in a 500 ks exposure. The red curves represent the best blackbody fit to the observational data (the model parameters are given in the bottom panel).

(minutes-hours) or long (months-years) time scales, and they are much higher than the optical fluxes, $f_x/f_{\text{opt}} \gtrsim 10^3$. Such properties strongly suggest that these objects are isolated, nearby NSs. Rotational periods in J0720.4–3125 and J1308.8+2127 were discovered with *ROSAT* and *Chandra*, respectively (see refs. in Table 2). There are also indications on periodicities in J0420.0–5022 and J0806.4–

4123, although those periods are to be confirmed yet. The source powering the thermal radiation of these NSs has been a matter of debate (e.g., Treves et al. 2000). Two main options under consideration are the internal heat of a cooling NS and accretion from the interstellar medium (ISM). A standard estimate on the luminosity powered by the Bondi-Hoyle accretion, $L_x \sim 2 \times 10^{31} n v_{10}^{-3} \text{ erg s}^{-1}$ (here n is the number density of the ISM in cm^{-3} , v_{10} is the relative NS velocity in units of 10 km s^{-1}), requires rather low NS velocities. Recent estimates on the distance to J1856.4–3754 and its proper motion (see below) imply a transverse velocity $v_{\perp} \simeq 185 \text{ km s}^{-1}$. Therefore, accretion cannot be the energy source for this object unless the star moves in a surprisingly dense medium (a cloud?) with $n \sim 10^2 \text{ cm}^{-3}$. First estimates of period derivatives for J0720.4–3125 (Zane et al. 2002; Kaplan et al. 2002b) and J1308.8+2127 (Hambaryan et al. 2002) imply surface magnetic fields² $\sim 10^{13} - 10^{14} \text{ G}$, which favors models invoking young (or middle-aged) cooling NSs rather than accreting NSs.

Below we present results from *Chandra* observations of the most famous (and best-investigated) objects of this class, J1856.5–3754 and J0720.4–3125.

4.1. RX J1856.5–3754

This object (we will call it J1856 throughout this Section) was first observed with *Chandra* in March 2000 in

² We note that these results are preliminary and require further confirmation.

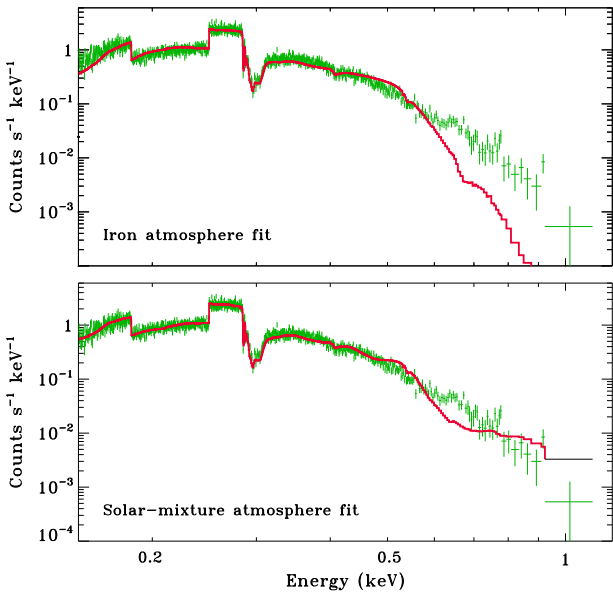


Fig. 19. Fits to the LETG spectrum of RX J1856.5–3754 to NS atmosphere models of heavy-element compositions assuming that the NS is a fast rotator (the models are from ZP02).

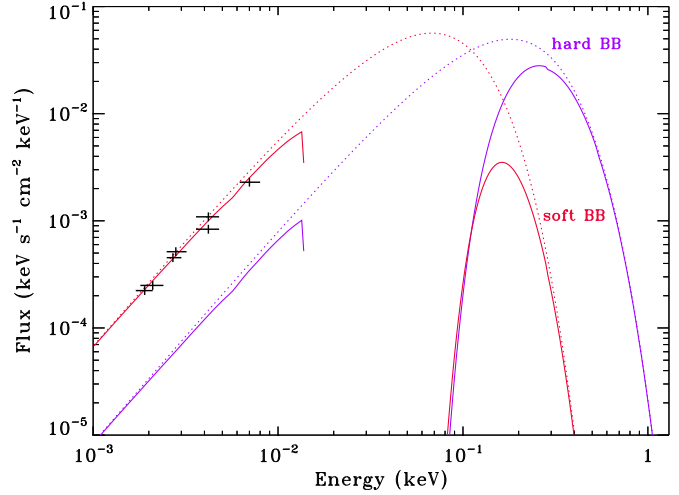


Fig. 20. Spectral flux of RX J1856.5–3754 as given by the best blackbody fit to the LETG data (blue curves, marked “hard BB”), with $T_{\text{bb}}^{\infty} = 0.73 \text{ MK}$ and $R_{\text{bb}}^{\infty} = 4.4 (d/120 \text{ pc}) \text{ km}$. The red curves give an example of a blackbody fit with $T_{\text{bb,s}}^{\infty} = 0.30 \text{ MK}$ and $R_{\text{bb,s}}^{\infty} = 18.2 (d/120 \text{ pc}) \text{ km}$ (“soft BB”) to the optical data (crosses). Solid curves show the absorbed spectra at $n_{\text{H}} = 1.0 \times 10^{20} \text{ cm}^{-2}$ (dots are the unabsorbed models).

a 55 ks exposure with the HRC-S/LETG instrument. A detailed analysis of this observation is given by Burwitz et al. (2001), who reported no detection of any significant features in the high-resolution spectrum. They also concluded that the combined X-ray and optical data rule out all the available NS atmosphere models: light-element models overpredict the actual optical fluxes (as first estimated by Pavlov et al. 1996), whereas heavy-element models do not fit the LETG spectrum. In October 2001 this source was observed for 450 ks, with the same instrument. However, even this very deep observation revealed no spectral features. The spectrum excellently fits a blackbody model of $T_{\text{bb}}^{\infty} = 0.73 \text{ MK}$ and $R_{\text{bb}}^{\infty} = 4.4 (d/120 \text{ pc}) \text{ km}$,³ with the hydrogen column density of $n_{\text{H}} = 1.0 \times 10^{20} \text{ cm}^{-2}$ (Fig. 18; see also Drake et al. 2002).

All attempts to find pulsations from J1856 have been unsuccessful so far (e.g., Ransom et al. 2002). However, since time resolution of both the *ROSAT* and *Chandra* data on J1856 was not sufficient to search for periods shorter than $\approx 10 \text{ ms}$, one could assume that the period of J1856 is shorter than that. Such a hypothesis might also explain the featureless spectrum of J1856 — spectral lines in radiation of a fast-rotating NS can be smeared out

³ The distance to J1856, $d \simeq 120 \text{ pc}$, has been recently established by Kaplan et al. (2002a) and Walter & Lattimer (2002).

because of the Doppler effect (rotational broadening; see ZP02 for more details). However, atmosphere models for a fast-rotating NS fail to fit the detected spectrum because of strong deviations at energies around most prominent absorption edges (see Fig. 19 and Fig. 12 in ZP02).

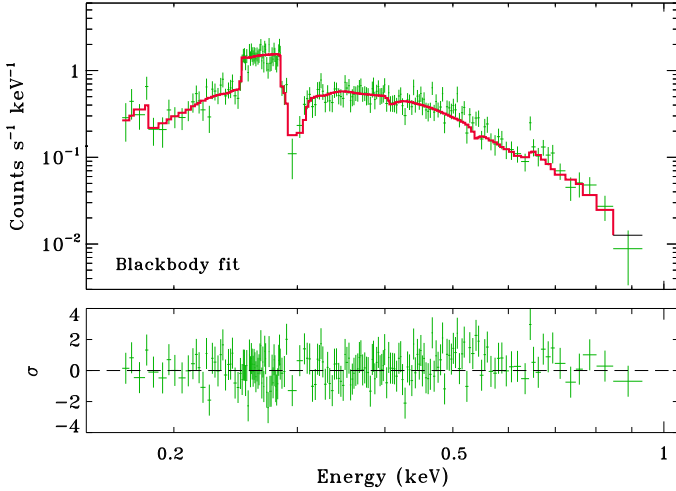


Fig. 21. *Chandra* LETG spectrum of RX J0720.4–3125. The red curve shows the best blackbody fit to the observational data (model parameters are given in the text).

Thus, we have to admit that the blackbody spectrum is the best model for the X-ray spectrum of J1856. In principle, such a blackbody spectrum could mimic the actual spectrum in the relatively short band of 0.15–1.0 keV if the NS surface is in a condensed form (according to Lai & Salpeter 1997, this can happen if the magnetic field is very strong at the NS surface, $B \gtrsim 10^{14}$ G). However, the radius of the emitting area, $R_{\text{bb}}^{\infty} \simeq 4\text{--}5$ km, is too small to be the NS radius. Moreover, taking into consideration the optical fluxes detected from J1856 (van Kerkwijk & Kulkarni 2001a; Pons et al. 2002), one encounters one more problem — the extrapolation of the blackbody model inferred from the X-ray data into the optical band falls well below the actually detected fluxes. One may assume (Pons et al. 2002) that the X-ray radiation is emitted from a hot area on the NS surface, while the optical radiation is emitted from the rest of the surface, with a lower temperature. The optical spectrum is well described by the Rayleigh-Jeans law (van Kerkwijk & Kulkarni 2001a) and gives the following relation between the temperature and the radius of the NS surface emitting the soft blackbody radiation: $R_{\text{bb},s}^{\infty} \simeq 8.3 (T_{\text{bb},s}^{\infty}/1 \text{ MK})^{-1/2} (d/100 \text{ pc})$ km (with allowance for the contribution of the “hard blackbody”). On the other hand, a 3σ upper limit on the temperature of the soft component, $T_{\text{bb},s}^{\infty} < 0.39$ MK, found from the X-ray data, corresponds to a lower limit for the radius $R_{\text{bb},s}^{\infty} > 16.3$ km for $d = 120$ pc. Figure 20 shows an example of the two-blackbody fit to the optical and X-ray data

on J1856. In this two-temperature picture, it is tempting to interpret the hot area as a pulsar polar cap. This seems to be consistent with the recent discovery of the H_{α} nebula surrounding J1856 (van Kerkwijk & Kulkarni 2001b), presumably a bow shock in the ambient medium created by the supersonic motion of a NS with a relativistic (pulsar?) wind. However, the hot spot is unusually large and luminous [$L_{\text{bol}}^{\infty} = 4 \times 10^{31} (d/120 \text{ pc})^2 \text{ erg s}^{-1}$] for a standard pulsar polar cap. This could be explained by a very strong magnetic field localized in the spot region (i.e., essentially different from a centered dipole). Such a field can quench the pair cascade in the wind of primary particles pulled out from the NS surface, which explains the lack of X-ray/optical synchrotron radiation. On the other hand, the strong field can increase the heat flux from the core/crust to the surface. The large size of the hot spot, together with the GR effects (ZP02), can explain the nondetection of pulsations (pulsed fraction $f_p \lesssim 4\%$ from the *Chandra* data), particularly if the hot spot is close to the rotational pole or the direction of the rotational axis is close to the line of sight. If the new observation of J1856 with *XMM-Newton* (conducted in April 2002) reveals pulsations of this objects, it will support the two-temperature interpretation and provide constraints on the magnetic moment, hot spot position and inclination of the rotational axis.

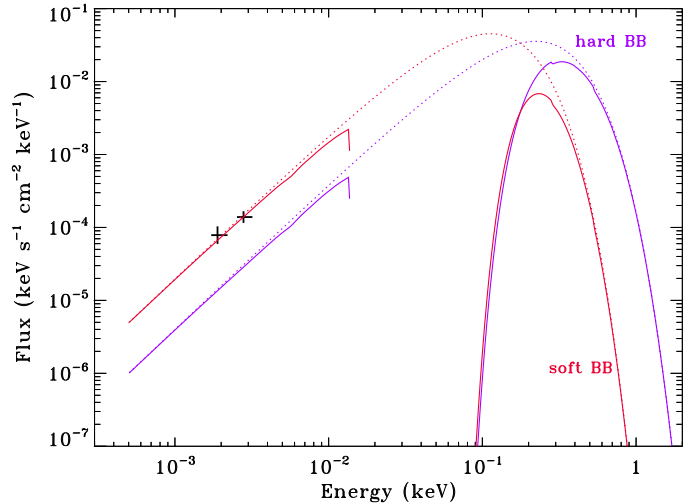


Fig. 22. The same as in Fig. 20, for RX J0720–3125. The parameters for the model spectra are given in the text. The optical data (crosses) are from Kulkarni & van Kerkwijk (1998).

4.2. RX J0720.4–3125

Chandra observed this object in February 2000 for 38 ks with the HRC-S/LETG instrument. Fitting various spectral models to these data gives results remarkably similar to those for J1856. Although the light-element (hydrogen and helium) NS atmosphere models provide acceptable fits (but the models are somewhat harder than the observed spectrum at $E > 0.75$ keV), the predicted optical fluxes (e.g., $B = 23.7$ and 23.3 for the hydrogen and helium nonmagnetic models, respectively) are much brighter than observed ($B \simeq 26.6$ — see Kulkarni & van Kerkwijk 1998). Neither iron nor solar-mixture models fit the data because of numerous features in the model spectra. The best fit is provided by a blackbody model of $T_{\text{bb}}^{\infty} = 0.92$ MK and a radius of the emitting area of $R_{\text{bb}}^{\infty} = 2.2 (d/100 \text{ pc})$ km, absorbed with the hydrogen column density $n_{\text{H}} = 1.7 \times 10^{20} \text{ cm}^{-2}$ (Fig. 21). However, similar to J1856, the best blackbody model inferred from the X-ray data underpredicts the optical fluxes which can be interpreted as emitted by a “soft blackbody” with $R_{\text{bb},s}^{\infty} \simeq 4.3 (T_{\text{bb},s}^{\infty}/1 \text{ MK})^{-1/2} (d/100 \text{ pc})$ km. To obtain an acceptable fit of the two-blackbody model to the X-ray data, one should keep $T_{\text{bb},s}^{\infty} \lesssim 0.50$ MK, that results in $R_{\text{bb},s}^{\infty} \gtrsim 6.1 (d/100 \text{ pc})$ km. Figure 22 shows an example of the two-blackbody fit to the optical and X-ray data, with $T_{\text{bb},s}^{\infty} = 0.45$ MK and $R_{\text{bb},s}^{\infty} = 6.4 (d/100 \text{ pc})$ km for the soft component. If future optical observations provide the distance to J0720.4–3125, it will be possible to evaluate the NS radius and, based on the X-ray light curves, estimate the mass-to-radius ratio.

5. Concluding remarks

Because of the limited space, we described the observational results on only a handful of observed thermally emitting isolated NSs. We only briefly mentioned AXPs and SGRs, whose X-ray radiation almost certainly contains a thermal component, with temperatures of 5–10 MK and equivalent radii of 1–5 km. The current status of AXPs, including their comparison with SGRs, is reviewed by S. Mereghetti et al. (this volume). From the observational perspective, the nature of these enigmatic objects can hardly be understood without deep multiwavelength observations, particularly in the IR and hard X-ray bands, which would help elucidate the origin of the nonthermal component and separate the thermal component more precisely. We did not touch “elderly” nearby pulsars (e.g., B1929–10, B0950+08), mostly because they have not been observed with *Chandra*. If future deep observations show that their X-ray radiation is indeed thermal (emitted from hot, small polar caps), as suggested by the *ROSAT* and *ASCA* observations, the analysis of the spectra and light curves will help establish the strength and geometry of their magnetic fields and the NS mass-to-radius ratio. We did not mention important non-detections of thermal radiation from very young pulsars, the Crab (Tennant et al.

2001; M.C. Weisskopf, this volume) and the recently discovered PSR J0205+6449 in the SNR 3C 58 (Slane et al. 2002), which put upper limits on the NS surface temperature. Finally, very interesting results on thermal radiation from transiently accreting NSs in quiescence have been reported recently (Rutledge et al. 2001, and references therein). Although these old NSs are not truly isolated, their radiation in quiescence resembles that of young isolated NSs because of additional heating due to pycnonuclear reactions in the compressed accreted material.

The *Chandra* observations described above have shown a few important things. First of all, they left no doubts that thermal emission indeed dominates in the soft X-ray radiation of quite a few isolated NSs, and the analysis of this radiation allows one to measure the NS temperatures⁴ and, in some cases, the radii or mass-to-radius ratios. Particularly important is the conclusion that the simple picture of a NS with a centered dipole magnetic field and uniform surface temperature is, most likely, an oversimplification. We see that whenever the data allow a detailed analysis, the temperature is not uniform, in both active pulsars and radio-quiet NSs. Moreover, the radius of X-ray emitting area is, as a rule, considerably smaller than the “canonical” NS radius. The example of J1210–5226 (Sec. 3.1) shows that the characteristic age ($\tau_c = P/2\dot{P}$) of a pulsar can differ from its true age by a large factor, and the conventional “pulsar magnetic field” can be quite different from the actual magnetic field at the NS surface. Therefore, any inferences on the properties of NSs and the superdense matter obtained without taking this into account should be considered with caution. For example, adopting the X-ray emitting radius to be the NS radius, a number of authors hurried to conclude that NSs are strange quark stars. Another example is the numerous comparisons of the NS cooling curves with observations of thermal X-rays from pulsars postulating that the pulsar’s characteristic age is the true age and the empirical temperature of one of the “thermal components” is a single effective temperature. If we want to understand the real objects, we should abandon the naive paradigm and answer the basic questions raised by the observations:

- What is the true explanation of the small, hot areas in many, if not all, NSs, such as J2323+5848 (CCO of Cas A), RX J1856.5–3754, etc? If these small heated areas are associated not with (unseen) pulsar activity, but with superstrong local magnetic fields, how such fields affect the thermal evolution of NSs?
- What is the relation between the various kinds of NSs — CCOs, AXPs, SGRs, active pulsars, dim NSs? For instance, why do CCOs, AXPs and SGRs show similar properties of thermal radiation, being so different in the other observational manifestations? Can it be that the mem-

⁴ See Fig. 5 in Mereghetti et al. (this volume) which demonstrates current estimates for the temperatures and luminosities of 22 thermally emitting NSs.

bers of different subclasses are intrinsically similar objects at different stages of their evolution (e.g., AXPs are descendants of CCOs) or viewed from different directions (e.g., dim NSs are usual middle-aged pulsars whose pulsar radiation is not seen because of unfavorable geometry)?

- What is the actual temperature distribution over the NS surface? Does the two-component model for thermal radiation we have used (thermal soft + thermal hard) describe the distribution adequately?
- What is the actual mechanism(s) of the surface emission? Are there any gaseous atmospheres at all? Why does the blackbody model describes the observed spectra so well in many cases?

These are the questions to be addressed (and, hopefully, answered) by future observations of NSs.

Acknowledgements. We gratefully acknowledge the support by the Heraeus foundation and the hospitality of the Physikzentrum Bad Honnef. The work of GGP and DS was partly supported by NASA grant NAG5-10865 and SAO grants GO2-3089X, GO2-3088X and SP2-2001C. We thank Marcus Teter and Vadim Burwitz, who participated in the analysis of some of the above-described *Chandra* observations.

References

- Becker W., Pavlov G.G., 2002, in *The Century of Space Science*, eds. J. Bleeker, J. Geiss & M. Huber (Dordrecht: Kluwer), in press
- Becker W., Trümper J., 1993, *Nature*, 365, 528
- Becker W., Trümper J., 1997, *A&A*, 326, 682
- Brinkmann W., Ögelman H., 1987, *A&A*, 182, 71
- Burwitz V., Zavlin V.E., Neuhäuser R., Predehl P., Trümper J., Brinkman A.C., 2001, *A&A*, 379, L35
- Caraveo P.A., De Luca A., Mignani R.P., Bignami G.F., 2001, *ApJ*, 561, 930
- Fahlman G.G., Gregory P.C., 1981, *Nature*, 293, 202
- Cheng A.F., Helfand D.J., 1983, *ApJ*, 271, 271
- Córdova F.A., Hjellming R.M., Mason K.O., Middleditch J., 1989, *ApJ*, 345, 451
- Drake J.J., Marshall H.L., Dreizler S., Freeman P.E., Fruscione A., Juda M., Kashyap V., Nicastro F., Pease D.O., Wargelin B.J., Werner K., 2002, *ApJ*, in press
- Giacani E.B., Dubner G.M., Green A.J., Goss W.M., Gaensler B.M., 2000, *AJ*, 119, 281
- Gould D.M., Lyne A.G., 1998, *MNRAS*, 301, 235
- Haberl F., Zavlin V.E., 2002, *A&A*, in press (astro-ph/0205460)
- Haberl F., Motch C., Buckley D.A.H., Zickgraf F.J., Pietsch W., 1997, *A&A* 326, 662
- Haberl F., Motch C., Pietsch W., 1998, *Astronom. Nach.*, 319, 97
- Haberl F., Pietsch W., Motch C., 1999, *A&A*, 351, L53
- Halpern J.P., Martin C., Marshall H.L., 1996, *ApJ*, 462, 908
- Hambaryan V., Hasinger G., Schwobe A.D., Schulz N.S., 2002, *A&A*, 381, 98
- Harding A.K., Strickman M.S., Gwinn C., McCulloch P., Mofet D., 2002, *ApJ*, in press (astro-ph/0205183)
- Helfand D.J., Becker R.H., 1984, *Nature*, 307, 215
- Helfand D.J., Gotthelf E.V., Halpern J.P., 2001, *ApJ*, 556, 380
- Kaplan D.L., van Kerkwijk M.H., Anderson J., 2002a, *ApJ*, 566, 378
- Kaplan D.L., Kulkarni S.R., van Kerkwijk M.H., Marshall H.K., 2002b, *ApJ*, 570, L79
- Kellett B.J., Branduardi-Raymont G., Culhane J.L., Mason I.M., Mason K.O., Whitehouse D.R., 1987, *MNRAS*, 225, 199
- Koptsevich A.B., Pavlov G.G., Zharikov S.V., Sokolov V.V., Shibanov Yu.A., Kurt V.G., 2001, *A&A*, 370, 1004
- Kouveliotou C., 1995, *Ap&SS*, 231, 49
- Kulkarni S.R., van Kerkwijk M.H., 1998, *ApJ*, 507, L49
- Lai D., Salpeter E.E., 1997, *ApJ*, 491, 270
- Marshall H.L., Shultz N., 2002, *ApJ*, in press (astro-ph/0203463)
- Mereghetti S., Bignami G.F., Caraveo P.A., 1996, *ApJ*, 464, 842
- Motch C., Haberl F., Zickgraf F.J., Hasinger G., Schwobe A.D., 1999, 351, 177
- Ögelman H., 1995, in *The Lives of the Neutron Stars*, eds. M.A. Alpar, Ü. Kiziloğlu and J. van Paradijs NATO ASI Ser. (Dordrecht: Kluwer), p.101
- Pavlov G.G., Stringfellow G.S., Córdova F.A., 1996, *ApJ*, 489, L75
- Pavlov G.G., Zavlin V.E., Trümper J., Neuhäuser R., 1996, *ApJ*, 472, L33
- Pavlov G.G., Welty A.D., Córdova F.A., 1997, *ApJ*, 489, L75
- Pavlov G.G., Sanwal D., Garmire G.P., Zavlin V.E., Burwitz V., Dodson R.G., 2000, *AAS Meeting 196*, #37.04
- Pavlov G.G., Kargaltsev O.Y., Sanwal D., Garmire G.P., 2001a, *ApJ*, 554, L189
- Pavlov G.G., Zavlin V.E., Sanwal D., Burwitz V., Garmire G.P., 2001b, *ApJ*, 552, L129
- Pavlov G.G., Sanwal D., Garmire G.P., Zavlin V.E., 2002a, in *Neutron Stars in Supernova Remnant*, ASP Conf. Series, eds. P.O. Slane & B.M. Gaensler, in press (astro-ph/0112322)
- Pavlov G.G., Zavlin V.E., Sanwal D., Trümper J., 2002b, *ApJ*, 569, L95
- Pavlov G.G., Sanwal D., Teter, M.A., Zavlin, V.E., 2002c, *AAS Meeting 200*, #80.01
- Pons J.A., Walter, F.M., Lattimer J.M., Prakash M., Neuhäuser R., An P., 2002, *ApJ*, 564, 981
- Ransom S.M., Gaensler B.M., Slane P.O., 2002, *ApJ*, 570, L75
- Rutledge R.E., Bildsten L., Brown E.F., Pavlov G.G., Zavlin V.E. 2001, *ApJ*, 559, 1054
- Sanwal D., Pavlov G.G., Kargaltsev O.Y., Garmire G.P., Zavlin V.E., Burwitz V., Manchester, R.N., Dodson R., 2002a, in *Neutron Stars in Supernova Remnants*, eds. P.O. Slane and B.M. Gaensler, in press (astro-ph/0112164)
- Sanwal D., Pavlov G.G., Zavlin V.E., Teter M.A., 2002b, *ApJ*, submitted
- Sanwal D., Pavlov G.G., Zavlin V.E., Teter M.A., Tsuruta S., Manchester R.N., 2002c, *ApJ*, submitted
- Slane P.A., Helfand D.J., Murray S.S. 2002, *ApJ*, 571, L45
- Seward F.D., Charles P.A., Smale A.P., 1986, 305, 814
- Schwobe A.D., Hasinger G., Schwarz R., Haberl F., Schmidt M., 1999, *A&A*, 341, L51
- Tennant A.F., Becker W., Juda M., et al., 2001, *ApJ*, 554, L173
- Treves A., Turolla R., Zane S., Colpi M., 2000, *PASP*, 112, 297
- Tsuruta S., 1998, *Phys. Rep.*, 292, 1
- van Kerkwijk M.H., Kulkarni S.R., 2001a, *A&A*, 378, 986

- van Kerkwijk M.H., Kulkarni S.R., 2001b, *A&A*, 380, 221
- Vasisht G., Kulkarni S.R., Anderson S.B., Hamilton T.T., Kawai N., 1997, *ApJ*, 476, L43
- Walter F.M., Matthews L.D., 1997, *Nature*, 389, 358
- Walter F.M., Lattimer J.M., 2002, *ApJ*, submitted (astro-ph/0204199)
- Walter F.M., Wolk S.J., Neuhäuser R., 1996, *Nature*, 379, 233
- Zampieri L., Campana S., Turolla R., Chierigato M., Falomo R., Fugazza D., Moretti A., Treves A., 2001, *A&A*, 378, L5
- Zane S., Haberl F., Cropper M., Zavlin V.E., Lumb D., Sembay S., Motch S., 2002, *MNRAS*, in press
- Zavlin V.E., Pavlov G.G., 1998, *A&A*, 329, 583 [ZP98]
- Zavlin V.E., Pavlov G.G., 2002, this volume [ZP02]
- Zavlin V.E., Pavlov G.G., Trümper J., 1998, *A&A*, 331, 821
- Zavlin V.E., Pavlov G.G., Sanwal D., Trümper J., 2000, *ApJ*, 540, L25
- Zavlin V.E., Pavlov G.G., Sanwal D., Trümper J., Manchester R.N., Halpern J.P., Becker W., 2002, *ApJ*, 569, 894